# Comparison of eddy viscosity turbulence models and stereoscopic PIV measurements for a flow past rectangular-winglet pair vortex generator

Charbel Habchi, Mohammad Oneissi, Serge Russeil, Daniel Bougeard, Thierry Lemenand

Version of Record: https://www.sciencedirect.com/science/article/pii/S0255270121003305
Manuscript_67241bd0d7f56e68a72df179375c634f

# Comparison of eddy viscosity turbulence models and stereoscopic PIV measurements for a flow past rectangular-winglet pair vortex generator

Charbel Habchi[a], Mohammad Oneissi[b], Serge Russeil[c,*], Daniel Bougeard[c], Thierry Lemenand[d]

[a]*Notre Dame University-Louaize, Thermofluids Research Group, 1200 Zouk Mosbeh, Lebanon*

[b]*Lebanese Intrenational University, Mechanical Engineering Department, Beirut, Lebanon*

[c]*IMT Lille Douai, University of Lille, F-59000 Lille, France*

[d]*University of Angers, Polytech Angers, LARIS EA 7315, 49000 Angers, France*

## Abstract

Vortex generators (VG) are widely used in enhancing the heat transfer coefficients in heat exchangers due to the development of longitudinal and transverse vortices. Therefore, understanding the development of these vortices has a high importance for the design and optimization of heat exchangers. When using numerical simulations, the choice of an appropriate turbulence model that can better predict the flow structure downstream a VG is fundamental. In the present study, three-dimensional numerical simulations, with two different commonly used eddy viscosity turbulence models, are performed for channel flow fitted with rectangular-winglet pairs (RWP) vortex generators. The numerical results are compared to experimental data obtained by stereoscopic particle image velocimetry (SPIV). The shear-stress transport (SST) $\kappa$-$\omega$ model and the re-normalization-group (RNG) $\kappa$-$\varepsilon$ model

* Corresponding author.
Tel.: +33 3 27 71 23 88; fax: +33 3 27 71 29 15
Email address: serge.russeil@mines-douai.fr (S. Russeil)

are used for modeling turbulence. Validation is conducted by comparing the flow structure topology and velocity field obtained from numerical simulations to those obtained using the SPIV method. It is found that the SST $\kappa$-$\omega$ model is better than the RNG $\kappa$-$\varepsilon$ turbulence model in predicting the flow characteristics downstream the RWP.

## Keywords:

Rectangular winglet pair; vortex generator; longitudinal vortices; turbulence model; stereoscopic particle image velocimetry.

## Nomenclature

| | |
|---|---|
| $B$ | Channel width, m |
| $D_h$ | Hydraulic diameter, m |
| $Re$ | Reynolds number |
| $H$ | Channel height, m |
| $L$ | Channel length, m |
| $x$ | Streamwise distance, m |
| $y$ | Spanwise distance, m |
| $z$ | Normal distance from bottom wall, m |
| $U$ | Mean flow velocity, m $s^{-1}$ |
| $u$ | Flow velocity in $x$ direction, m $s^{-1}$ |
| $v$ | Flow velocity in $y$ direction, m $s^{-1}$ |
| $w$ | Flow velocity in $z$ direction, m $s^{-1}$ |

*Abbreviations*

| | |
|---|---|
| *CFD* | Computational Fluid Dynamics |
| *LDA* | Laser Doppler Anemometer |
| *LVG* | Longitudinal Vortex Generator |
| *PIV* | Particle Image Velocimetry |
| *RWP* | Rectangular Winglet Pair |
| *RNG* | Re-normalization Group |
| *SST* | Shear-Stress Transport |
| *TKE* | Turbulent Kinetic Energy |
| *TVG* | Transverse Vortex Generator |
| *VG* | Vortex Generator |

*Greek letters*

| | |
|---|---|
| $\mu$ | Dynamic viscosity, Pa s |
| $v$ | Kinematic viscosity, $m^2$ $s^{-1}$ |
| $\rho$ | Fluid density, kg $m^{-3}$ |
| $\Gamma_2$ | Gamma-2 function |
| $\kappa$ | Turbulence kinetic energy, $m^2$ $s^{-2}$ |
| $\varepsilon$ | Dissipation rate, $m^2$ $s^{-3}$ |
| $\omega$ | Specific dissipation rate, $s^{-1}$ |
| $\Sigma$ | Modulus of the mean strain rate tensor, $s^{-1}$ |

# 1. Introduction

Heat exchangers are involved in various applications starting from small household radiators to large chillers and condensers in power plants. Several active, passive and compound techniques were used in order to increase the thermal performance of heat exchangers while keeping relatively low pumping power [1, 2, 3, 4, 5, 6]. In particular, passive technique, and especially vortex generators (VG), is the most commonly studied method in enhancing heat exchangers due to many reasons such as their efficiency, easy manufacturing and maintenance [6, 7]. Passive VG exist in various shapes [8, 9], and they produce mainly two type of vortices, namely longitudinal vortices (LV) and transverse vortices (TV). TV are two-dimensional swirling flows with axes normal to the main flow direction, while LV rotate about an axis in the streamwise direction, implying a three-dimensional helicoid swirling motion. LV are found to have an advantage over TV in terms of scalar mixing and heat transfer performances [10, 11, 12].

In order to investigate the flow structure induced by these vortex generators, three methods are commonly used in the open literature: experimental measurements, theoretical developments and numerical simulations. While theoretical analysis is limited to very specific academic flow configurations, experiments in fluid mechanics are considered a very important part for investigating flow structure characteristics by using for instance laser Doppler velocimetry and particle image velocimetry (PIV) [13, 14, 15]. They can supplement and validate theoretical studies and numerical modelling of flow field downstream VG. Computational fluid dynamics (CFD) simulation is widely used in studying the formation and development of TV and LV downstream VG. Since experimental methods are very expensive, time consuming and involve too much labor, numerical simulation has become more and more popular with the advances in computational power [16, 17, 18]. CFD simulations are flexible; since adjusting computerized model is much easier and cheaper than real prototypes.

Moreover, CFD simulations can provide profound analysis; because one can analyze physically unreachable zones, in addition to shape optimization for heat transfer and mixing enhancement [12, 19, 20].

Consequently, numerous studies using numerical simulations have been carried in order to analyze the thermal and hydraulic performances of vortex generators in heat exchangers. These studies have an important industrial impact since the intensification of heat transfer using VGs allows significant performance increases. But most often the choice of the turbulence model is made by comparison on the overall performance of the exchanger which does not allow to precisely quantify the capacity of the computer code to accurately predict detailed features of the turbulent wake downstream VGs [21, 2].

Various turbulence models were used by the authors to model transverse and longitudinal vortices in turbulent flows. Two of the most commonly used turbulence models are the re-normalization-group (RNG) $\kappa$-$\varepsilon$ model [22, 23, 24] and the shear-stress transport (SST) $\kappa$-$\omega$ model [25, 26]. The RNG $\kappa$-$\varepsilon$ model is well known to improve the accuracy of the result in rapidly strained and swirling or rotating flows. The SST $\kappa$-$\omega$ model is known to be accurate for wide range of flows such as transonic shock waves and adverse pressure gradients and it performs very well in the near-wall region as well as in the flow core [27].

In simulating turbulent flows downstream VG, the selection of appropriate turbulence model plays a massive role in the prediction of the hydraulic performance and thus convective heat transfer. For this reason, and since the most used models for modeling turbulent flows downstream VG are the RNG $\kappa$-$\varepsilon$ and SST $\kappa$-$\omega$ models, this paper focuses on comparing these two models with an experimental study using stereoscopic PIV (SPIV).

In this study, we investigate longitudinal vortices generated by rectangular-winglet pairs in parallel plate turbulent channel flow to examine the flow structure characteristics. A row of rectangular winglet pairs is fixed in a parallel plate test bench channel. SPIV is used to harvest

three dimensional (3D) instantaneous velocity fields in the flow configuration for a Reynolds number $Re = 4000$ (based on the channel's hydraulic diameter) which is a typical value in the range of those commonly studied in the open literature. The dimensions of the test section and VG as well as the Reynolds number used here are commonly used in studies from the open literature [28].

The numerical method, computational domain and mesh sensitivity analysis are presented in Section 2. Section 3 is devoted for the experimental setup. Comparison between experimental and CFD simulations of flow topologies in horizontal and vertical planes are presented in Section 4. Section 5 is devoted to the concluding remarks.

## 2. Numerical Procedure

### 2.1 Governing equations and turbulence models

The flow is governed by the 3D steady-state Reynolds-averaged Navier-Stokes (RANS) equations computed using ANSYS Fluent 15 which is based on a cell-centered finite volume discretization method [24]. RANS turbulence modelling approach allows the calculation of the mean flow without first calculating the full time-dependent flow field. Two turbulence models are particularly detailed and used in this study.

First, the re-normalization-group (RNG) $\kappa$-$\varepsilon$ model was developed by Yakhot *et al.* [29, 30] using RNG method to renormalize the Navier-Stokes equations in order to capture the effects of small scale motion in a turbulent flow. In standard $\kappa$-$\varepsilon$ model, the turbulent diffusion is accounted only at a specific scale, since eddy viscosity is resolved from a single length scale. This trend is not realistic since all turbulence scales will contribute to the turbulent diffusion. The modified $\kappa$-$\varepsilon$ model solves this problem and involves different scales to the production term. The RNG $\kappa$-$\varepsilon$ model shows fundamental improvements over the

standard $\kappa$-$\varepsilon$ model and enhances the final solution [31], where the effects of turbulence of strong streamline curvature, vortices and swirl effects are taken in account [32].

Second, the shear-stress transport (*SST*) $\kappa$-$\omega$ model developed by Menter [33] is also used in this study. This model solves two partial differential equations: one for the turbulence kinetic energy equation $\kappa$ and the other for its specific dissipation rate $\omega$. Also, the shear-stress transport combines the use of $\kappa$-$\omega$ formulation in the inner parts of the boundary layer and the switching to a $\kappa$-$\varepsilon$ behavior in the free-stream thus avoiding the $\kappa$-$\omega$ sensitivity to the inlet free-stream turbulence properties. In addition, it is characterized by its good behavior in adverse pressure gradients and separating flows while attaining accuracy and reliability [34]. The preceding attributes give the SST $\kappa$-$\omega$ model additional accuracy and reliability thus providing it an advantage over the standard $\kappa$-$\omega$ model.The SST $\kappa$-$\omega$ model was used by many researchers in previous works proving a fair match with experimental results [35, 25]. This approach necessitates assessment of the wall adjacent cell size analogous to the dimensionless wall distance $y^+$ lower than 4, ensuring that the viscous sublayer is meshed.

Low Reynolds correction and near-wall treatment are adopted for the SST $\kappa$-$\omega$ and RNG $\kappa$-$\varepsilon$ turbulence models, respectively. Double precision and second order upwind numerical schemes are used for spatial discretization of the convective terms [36]. Central-difference and second order accuracy are used for the diffusion terms. The Coupled algorithm is used for the pressure-velocity coupling with the pseudo-transient option which is a form of implicit under-relaxation for steady-state cases. Pseudo-transient option allows the user to obtain solutions faster and more robustly. For detailed description of the different methods and model equations, the reader could refer to [34].

## 2.2 Computational domain and boundary conditions

The test section consists of one row of rectangular winglet pair vortex generators that produce pairs of main longitudinal vortices (see next section). This configuration allows to

assume two planes of symmetry; the first is at the channel midplane and the other at one side of the middle winglet pair. The channel streamwise direction is defined as $x$, spanwise direction as $y$ and $z$ for the vertical direction.

Figure 1 presents an isometric view showing the computational domain and boundary conditions. The channel height is $H$=37.8 mm with breadth $B$=1.6$H$ and length $L$=11$H$. Each rectangular winglet is 1.5$H$ in length, $H$/2 in height and thickness equals to 0.05$H$. The winglets are set normal to the channel bottom wall with an angle of attack of 30° from the incident flow, and the distance separating the leading edges of VG is 0.2$H$.

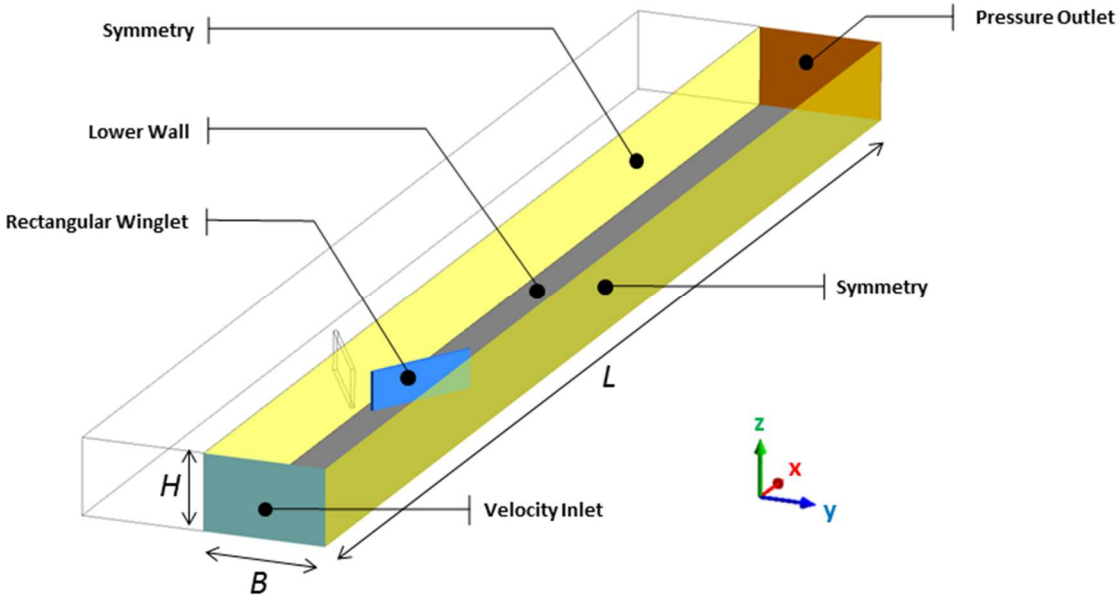


**Figure 1** Computational domain and boundary conditions.

The Reynolds number is calculated based on the channel hydraulic diameter $D_h = 2H$ and it is equal to $Re$=4400. To ensure the same incoming flow conditions, the inlet velocity profile function is extracted from the experimental measurement and then fitted with an analytical solution by means of a user defined function (UDF).

The analytical velocity profile used to fit the experimental inlet velocity is based on the model developed by Štigler [37] based on vorticity distribution between two parallel plates.

Štigler velocity profile fits realistic results better than the power law velocity profiles that was derived for pipe flows, since the derivative of the function does not tend to infinity at the boundaries, thus no infinite shear stress at the walls. In addition, Štigler analytical solution solves the Munson power law in which the derivative of the function at the middle of the channel does not tend to zero. Štigler's analytical profile is defined as [37]:

$$\frac{U}{U_{max}} = 1 - \left[\frac{|2z - H|}{H}\right]^{n+1} \tag{1}$$

$$n = \frac{H^2(P_1 - P_2)}{4L\mu U_{mean}} - 2 \tag{2}$$

where $U$ is the longitudinal velocity (m.s$^{-1}$), $U_{max}$ is the maximum velocity (m.s$^{-1}$), $H$ is the channel height (m), $z$ is the vertical distance from the bottom wall (m), $0 \leq z \leq H$, $n = 3.4$ is a pressure drop depending constant, $U_{mean}$ is the mean flow velocity (m.s$^{-1}$), $P_1 - P_2$ is the pressure drop (Pa) obtained from the friction factor inside an empty duct flow. This expression can be used for both laminar and turbulent velocity profiles.

## 2.3 Mesh sensitivity analysis

The mesh used in this work is similar to a previous study done by Oneissi *et al.* [28] in which a non-uniform mesh with polyhedral cells is adopted for the computational domain. All walls in the channel are treated with 10 inflation layers with 40 µm first layer thickness for attaining $y^+$ values less than 1. Table 1 presents the channel mesh characteristics used in this work. The mesh sensitivity analysis is done according to the method proposed by Celik *et al.* [38]. According to this method a grid convergence index $(GCI)$ is calculated for several flow parameters. In our study, we consider local velocity distribution in the wake of the VG as well as the pressure drop across the flow domain. Four mesh densities were studied as follows: 500,000 – 860,000 – 1,600,000 – 2,500,000. It is found that for a mesh size of around 2.5 million cells, the $GCI$ for local velocity did not exceed 1.2 % and the $GCI$ for the pressure

drop was lower than 0.7 %, for both eddy viscosity turbulence models. Thus, this mesh is adopted for the present numerical simulations.

To ensure good convergence of the results, the criteria are based on the continuity, linear momentum, and energy equations with residuals of at least $10^{-8}$.

**Table 1** Mesh characteristics

| | |
|---|---|
| **Maximum element size (mm)** | 1.30 |
| **Type of mesh** | Polyhedral |
| **Number of elements** | $2.5 \times 10^6$ |
| **Inflation (μm)** | 40 |
| **Inflation layers** | 10 |
| **Maximum $y^+$** | 0.40 |

## 3. Experimental Method

The experimental studies are performed in a close-loop air channel shown in Figure 2. The same experimental setup has been used in a previous study where more details are given on the benchmark and measurement method in Ref. [39]. In this paper we give a brief description of the experimental benchmark and method adopted.

The test section is 1200 mm in length, 500 mm in width and of height equal to 37.8 mm. The flow rate is controlled by varying the rotational speed of the fan. In the seeding room, seeding particles are generated through a controlled combustion process of which produces about 1 μm mean diameter smoke particles with a density around 1.06 kg/m$^3$ [40, 41] used as flow tracers. A row of rectangular winglet pair VG is mounted on the bottom wall and used to generate longitudinal vortices in the test channel. The test section consists of four rectangular winglet pairs. Only one pair of rectangular winglets at the middle of the test section is investigated in this study due to symmetric boundary conditions as explained in the previous section for the CFD study. The VG are manufactured by means of an Objet Alaris 30 Desktop 3D Printer using photopolymer jetting technology.

Stereoscopic PIV technique is used in this work and it consists of a laser light source, two digital cameras and image-based processing software. The three velocity field components are measured in two plane orientations:

• *xy* measurement planes, where the laser sheet is placed horizontally above the winglets row parallel to the bottom wall.

• *yz* measurement planes, where the laser sheet is placed vertically in cross-sections normal to the main flow direction at distinct locations.

In each measurement plane, 3000 images were captured with a sampling frequency of 2 Hz.

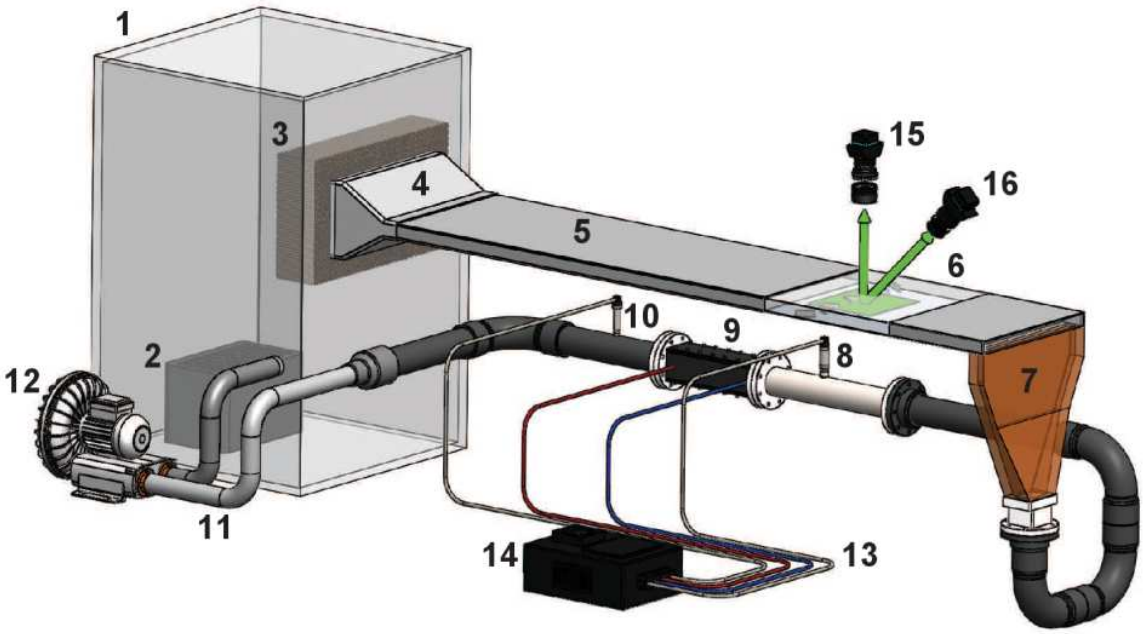


**Figure 2** Close-loop air channel setup: (1) Seeding room; (2) Particle generator; (3) Honeycomb; (4) Convergent section; (5) Upstream channel; (6) Test section (lateral and upper glazed windows); (7) Convergent 90°-elbow; (8) Absolute pressure transducer; (9) Laminar flowmeter; (10) Temperature probe; (11) PVC suction pipe; (12) Centrifugal fan; (13) Wirings and cables; (14) Micro-manometer and temperature recorder ; (15) Normal camera; (16) Inclined camera.

# 4. Results and discussion

## 4.1 Streamwise velocity profile

Before comparing the experimental and numerical findings, the mean flow velocity profile at the inlet cross section is presented in along with the analytical velocity profile obtained from Eq. (2) for $Re = 4400$. The experimental and analytical velocity profiles show a great agreement and can be used as an inlet boundary conditions for the CFD simulations. The average error between experimental and analytical velocities is less than 2%.

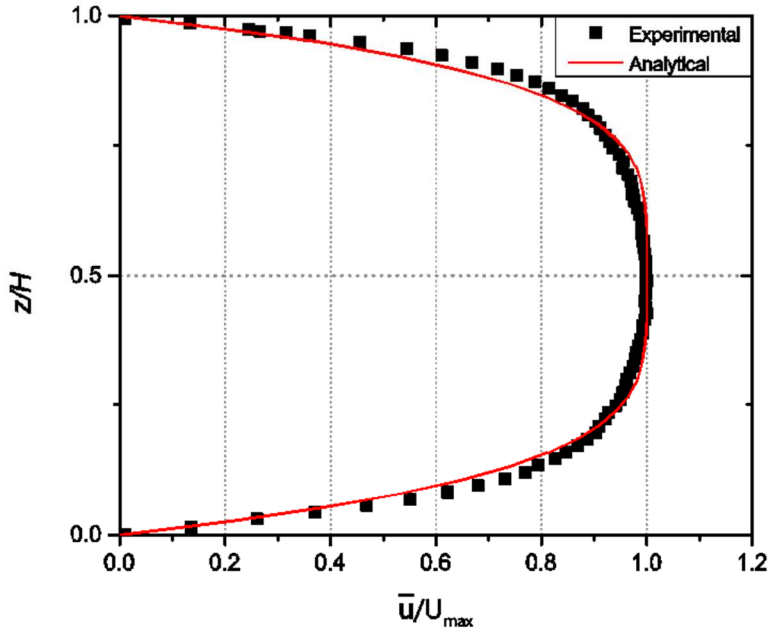


**Figure 3** Mean flow velocity at the inlet cross section from experimental and analytical methods.

In order to analyze the eddy viscosity turbulence models in predicting the generation and dissipation of longitudinal vortices generated by rectangular winglet pair, local comparison of the velocity field from CFD and SPIV measurements is conducted in this section. Measurements of longitudinal velocity profiles at a distance $x = H$ downstream the VG trailing edge and vertical distance $z$=24 mm from the bottom wall are compared for instance in Figure 3. This figure shows a comparison between longitudinal mean velocity profiles ($\bar{u}$) normalized by the bulk velocity ($U$) extracted from experimental results with a

7% error and from the two numerical simulations results. This error on experimental results is estimated from repeatability study performed on several days and various flow conditions. The normalized velocity profile ($\bar{u}/U$) obtained by numerical simulation using SST $\kappa$-$\omega$ turbulence model is in good agreement with experimental results. The average error between these simulation results and experimental results is less than 5% with a maximum error at the channel center line of about 12%.

Similar qualitative behavior of velocity profile is obtained for RNG $\kappa$-$\varepsilon$ turbulence model however it is quantitatively farther from the data obtained using SPIV and SST $\kappa$-$\omega$ model. Hence, the RNG $\kappa$-$\varepsilon$ turbulence model could not accurately predict the longitudinal velocity profile.

This type of comparison is not enough to judge or even validate the use of the SST $\kappa$-$\omega$ turbulence models. Further detailed comparison of the flow structure characterization and flow topologies are conducted in the next paragraphs by comparing the velocity field and turbulence kinetic energy at different cross-sectional positions.

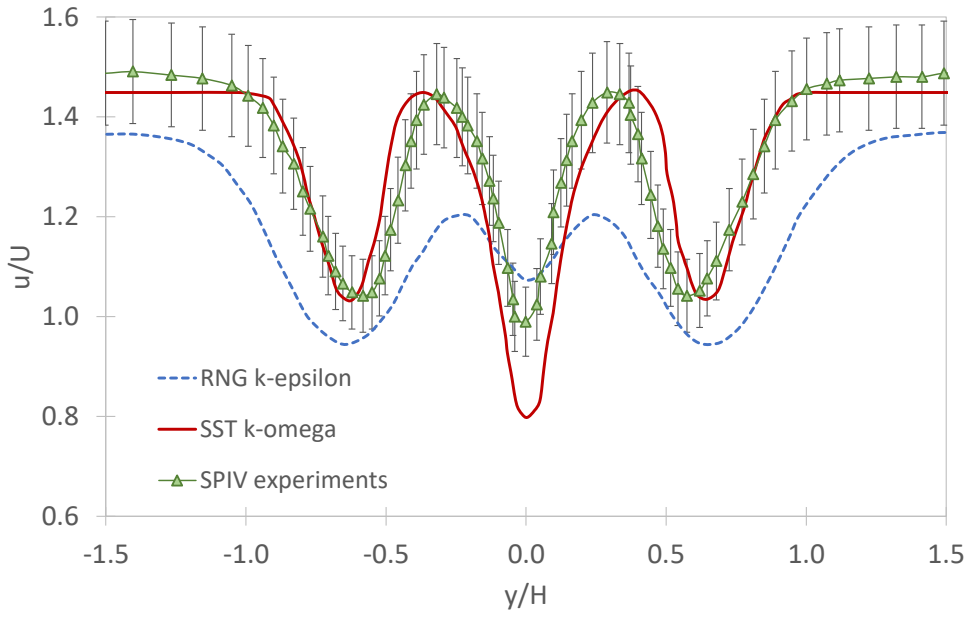

**Figure 3** Comparison between normalized mean velocity profiles extracted from experimental results (with 7% error) and numerical simulations, at $x/H$=1 downstream the VG trailing edge and vertical distance $z$=24 mm.

## 4.2 Horizontal velocity components

Flow structure in horizontal plane of both turbulence models are compared with SPIV experimental results in this section. In order to investigate the flow topology in the horizontal plane *xy* ($z$=24 *mm* from bottom wall), first, the three mean velocity components $\bar{u}$, $\bar{v}$ and $\bar{w}$ are compared with experimental results. Second, to investigate the turbulent characteristics of the flow, turbulent kinetic energy is also compared.

### *4.2.1 Comparison between SPIV and RNG κ-ε turbulence model*

Results obtained by numerical simulation and experimental method are post-processed using Matlab adopting similar image filtering and colormaps. Figure 4 presents comparison of mean velocity components ($\bar{u}$, $\bar{v}$, $\bar{w}$) in horizontal plane from experimental data and numerical results obtained using RNG $\kappa$-$\varepsilon$ turbulence model at $Re$=4400 and at a position $z$=24 mm from bottom wall.

For the mean longitudinal velocity ($\bar{u}$), different velocity topologies are observed between experiment and simulation. The topologies of the mean transverse velocity component ($\bar{v}$) obtained from experimental and numerical results are not in good agreement with SPIV results. Figure 4 (b) shows that the transverse velocity component ($\bar{v}$) is totally trapped in region directly in the wake of the winglet pair in which it dissipates rapidly after a distance $x/H$=4. This means that the main vortex is quickly dissipated which is not the case shown by SPIV results. The vertical component ($\bar{w}$) obtained by CFD is shown in Figure 4 (c) and do not show good correspondence with experimental results. It can be observed that the RNG $\kappa$-$\varepsilon$ turbulence model could not predict the induced vortices and only one stagnation

zone line is predicted in the lower half unlike experimental data. Only the main vortex is predicted by the RNG $\kappa$-$\varepsilon$ turbulence model produced due to flow separation over the winglet and rotates in a clockwise (CW) direction. This main vortex vanishes quickly in the CFD simulations while SPIV results show that it persists to longer distance downstream the VG.

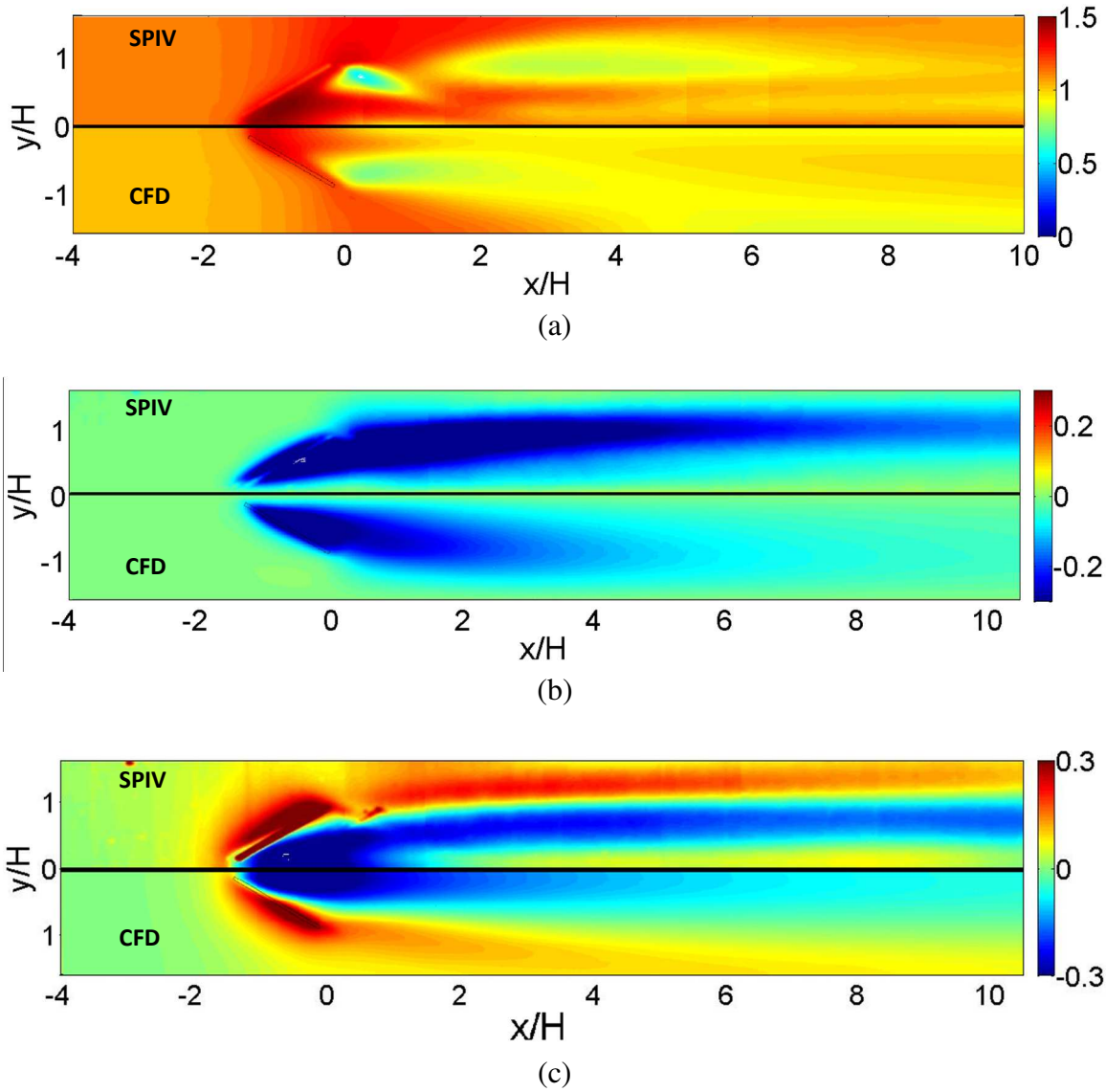


(a)

(b)

(c)

**Figure 4** Comparison of mean flow velocity components in the horizontal plane at *Re*=4400 and $z$=24 mm from bottom wall: (a) $\overline{\boldsymbol{u}}$, (b) $\overline{\boldsymbol{v}}$, (c) $\overline{\boldsymbol{w}}$, upper section from experimental results and lower section from numerical simulations using RNG $\kappa$-$\varepsilon$ turbulence model.

Figure 5 presents a comparison of the normalized turbulent kinetic energy between experimental results and numerical simulation using RNG $\kappa$-$\varepsilon$ turbulence model at $Re$=4400 and $z$=24 mm from bottom wall. Both figures are totally unsymmetrical with no good correspondence between CFD and SPIV results. Hence, the RNG $\kappa$-$\varepsilon$ turbulence model could not predict the turbulent kinetic energy even in an approximate manner.

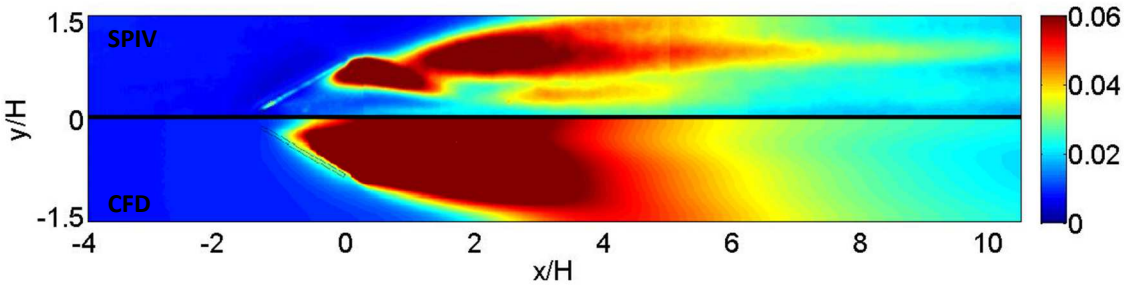


**Figure 5** Comparison of the normalized turbulent kinetic energy topologies at $Re$=4400 and $z$=24 mm from bottom wall, between experimental results (upper section) and numerical simulation using RNG $\kappa$-$\varepsilon$ turbulence model (lower section).

### *4.2.2 Comparison between SPIV and SST $\kappa$-$\omega$ model*

A similar strategy is followed in this section for comparing CFD using SST $\kappa$-$\omega$ turbulence model and experimental results. Figure 6 compares the contours of velocity components in the horizontal plane. On each figure, the upper half of the image represents the experimental results obtained by SPIV, while the bottom half presents contours obtained from numerical simulation, indicated by CFD.

From the CFD contours of the mean longitudinal velocity $\bar{u}$, the maximum values occur above the rectangular winglet pair and different areas of velocity variation are observed in the wake. The main two areas of velocity deficit are associated to the evolution of longitudinal vortices in the wake region of each rectangular winglet. The same phenomenon can be observed near the symmetric axis after a distance $x/H$=2 corresponding to the development of

the induced vortices. The CFD results are in very good agreement with contours depicted from the SPIV method. The topologies of the mean transverse velocity component $\bar{v}$ obtained from experimental and numerical results are also compared in Figure 6 (b). It is observed that the transversal velocity component $\bar{v}$ is embedded in region behind the winglet pair in the wake due to flow separation and dissipates along the channel in a manner similar to experimental data. Figure 6 (c) shows the vertical component $\overline{w}$ obtained by CFD and experiments and show a great correspondence between both methods. It can be observed that the flow is directed downward in the symmetry plane and then splits into two regions: two main longitudinal vortices in the two regions separated by *y/H*=0 axis. In each region, the up-wash flow is colored in red, the downwash effect is colored in blue and zero velocity is colored in green. A main vortex is produced due to flow separation over the winglet and rotates in a clockwise (CW) direction and an induced vortex rotating counterclockwise (CCW) is beginning to develop after a distance *x/H*=2 from winglet trailing edge. Both, experimental and numerical results are in excellent correspondence with each other and show almost non-distinguishable flow topologies.

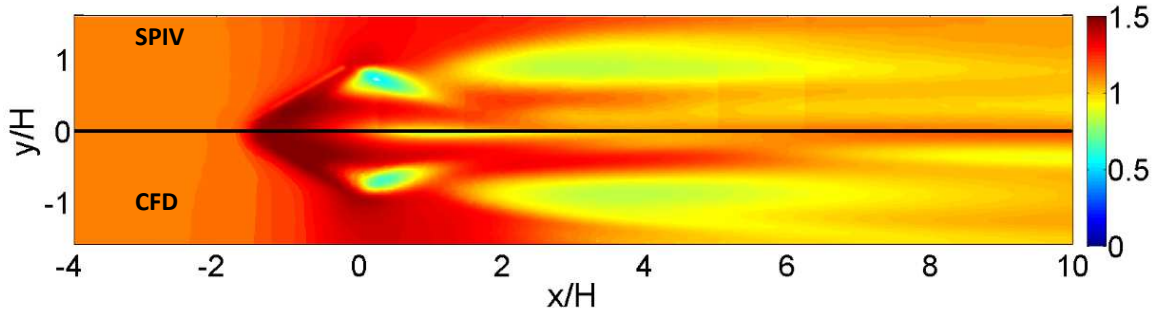

(a)

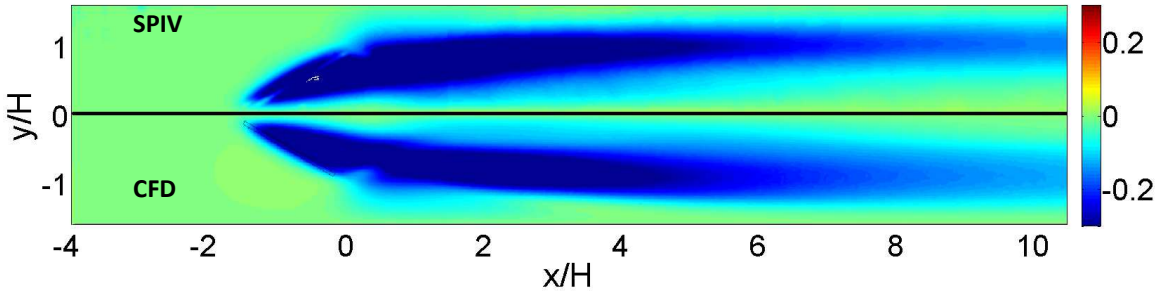


(b)

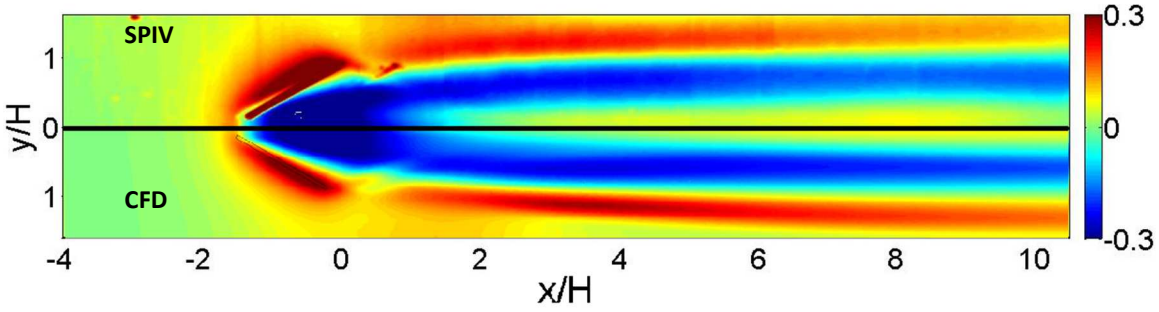


(c)

**Figure 6** Comparison of mean flow velocity components in the horizontal plane at *Re* = 4400 and *z*=24 mm from bottom wall: (a) $\overline{\boldsymbol{u}}$, (b) $\overline{\boldsymbol{v}}$, (c) $\overline{\boldsymbol{w}}$, upper section from experimental results and lower section from numerical simulations using SST $\kappa$-$\omega$ turbulence model.

Figure 7 shows a comparison of the turbulent kinetic energy profiles, normalized with the square of mean flow velocity ($U^2$), between experimental results (denoted by SPIV) and numerical simulation using SST $\kappa$-$\omega$ turbulence model at *Re*=4400. Both figures are not perfectly superposing, but they are in relatively good agreement. SST $\kappa$-$\omega$ turbulence model seems to have good agreement with experimental results for the turbulence kinetic energy of the primary vortex however, it does not reproduce fairly that for secondary vortex, especially from *x*/*H* higher than 3. Meanwhile, the effectiveness of the SST $\kappa$-$\omega$ is much better than the RNG $\kappa$-$\varepsilon$ model as concluded from these two last sections.

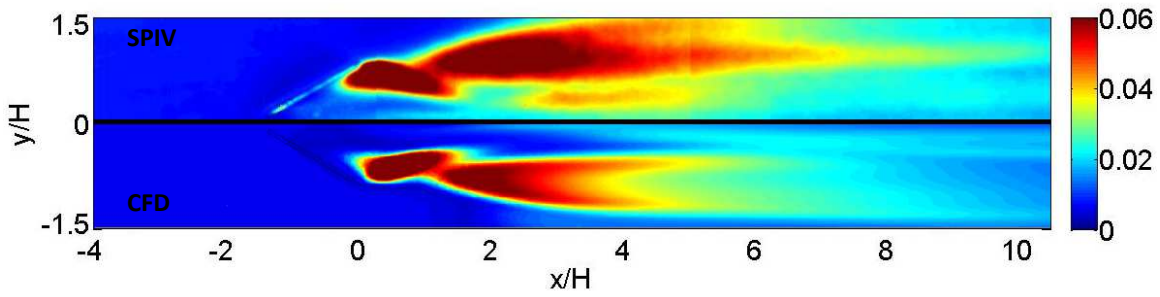


**Figure 7** Comparison of the normalized turbulent kinetic energy topologies at *Re*=4400 and *z*=24 mm from bottom wall, between experimental results (upper section) and numerical simulation using SST $\kappa$-$\omega$ turbulence model (lower section).

### 4.3 Secondary flow structure

In addition to the flow field comparison in horizontal plane, flow topologies in vertical planes are extracted for further examination of the turbulence models prediction of longitudinal vortices at several locations in the wake region. In this section, $\Gamma_2$ criterion proposed by Favelier *et al.* [42] and employed previously by Oneissi *et al.* [39] to identify and track the main and induced vortices in cross sections downstream the winglet pair, is also used here to validate turbulence model predictions. Comparing topologies of the $\Gamma_2$ criterion with SST $\kappa$-$\omega$ turbulence model and RNG $\kappa$-$\varepsilon$ turbulence model at different locations ($x$= $H$, 3$H$, 5$H$, 9$H$ and 10.5$H$) are respectively illustrated in Figure 8 and Figure 9. The results are presented in a symmetrical manner for better visibility.

It is clearly shown from Figure 8 that the SST $\kappa$-$\omega$ turbulence model accurately predicts and identifies the generated vortices location at different vertical planes, while Figure 9 shows that the RNG $\kappa$-$\varepsilon$ turbulence model could not predict the generation of these streamwise vortices which are the most responsible for macromixing and heat transfer enhancement [6, 11].The RNG $\kappa$-$\varepsilon$ turbulence model only predicts the formation of one main vortex that develops along the channel, but it fails in predicting any induced vortices. Whereas, the SST $\kappa$-$\omega$ turbulence model predicts precisely the number of generated vortices and the relative

position of these vortices. Figure 8 shows that SST $\kappa$-$\omega$ turbulence model predicts one main vortex in addition to two induced vortices near the bottom wall of the channel at a distance $x=H$. Also, for the other planes, the SST $\kappa$-$\omega$ turbulence model predicts accurately the main and induced vortices numbers and locations.

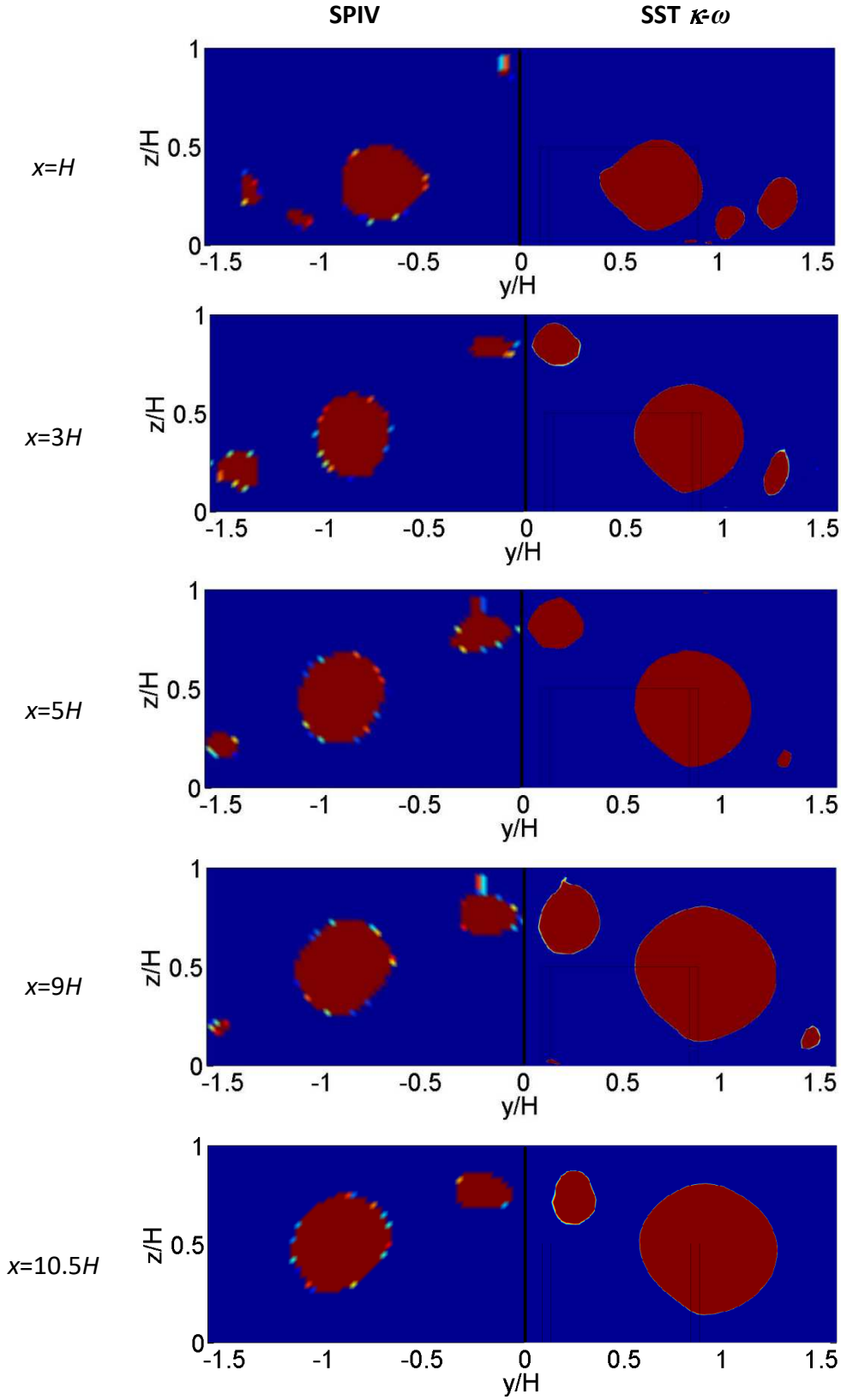


**Figure 8** Comparison of $\Gamma_2$ function topologies used for vortex identification downstream the winglet pair at *Re*=4400 between experimental results (left section) and numerical simulation using SST $\kappa$-$\omega$ turbulence model (right section).

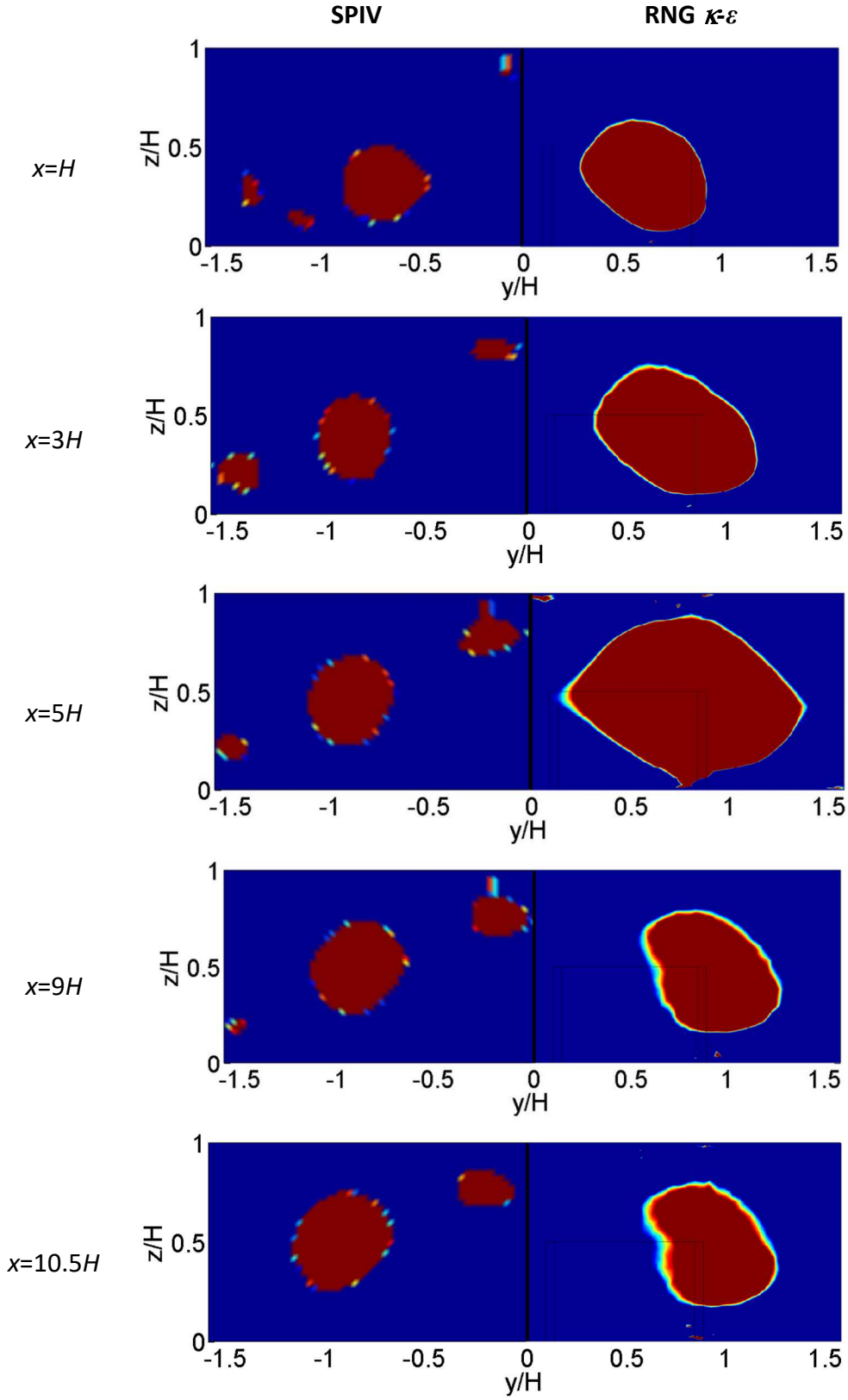


**Figure 9** Comparison of $\Gamma_2$ function topologies used for vortex identification downstream the winglet pair at *Re*=4400 between experimental results (left section) and numerical simulation using RNG $\kappa$-$\varepsilon$ turbulence model (right section).

## 5. Conclusion

In this study, a comparison between CFD numerical simulation and SPIV experimental data of longitudinal vortices generated downstream rectangular winglet pairs in parallel plate-fin channel is investigated at a Reynolds number $Re$=4400. Two eddy viscosity models are adopted, namely the RNG $k-\epsilon$ and SST $k-\omega$ turbulence models, which are the most widely used when dealing with flow and heat transfer downstream vortex generators.

The aim of this study is to qualify turbulence model in predicting the flow structure of longitudinal vortices in a parallel plate channel, since these vortices are the most responsible for macromixing and heat transfer enhancement. The obtained results of the velocity profile from the simulations are compared locally with experimental data extracted using SPIV techniques. Local velocity profile in the wake of the VG obtained from the SST $\kappa$-$\omega$ turbulence model shows a good correspondence with experimental data, while RNG $\kappa$-$\varepsilon$ turbulence model did not predict well the same behavior.

Velocity fields on a horizontal flow sections in addition to the turbulent kinetic energy distribution are inspected. The SST $\kappa$-$\omega$ turbulence model shows fair agreement with experimental results. On the other hand, the RNG $\kappa$-$\varepsilon$ turbulence model shows no consistency at all with experimental results. Meanwhile, the SST $\kappa$-$\omega$ turbulence model is found to not accurately predict the turbulent kinetic energy of the induced secondary vortex.

The flow topology is also compared on several cross sections downstream the VG to show development and number of streamwise vortices by means of $\Gamma_2$ criterion. The SST $\kappa$-$\omega$ turbulence model accurately predicts and identifies the generated vortices location at different planes, the number of generated vortices (main and induced) as well as their relative positions. The RNG $\kappa$-$\varepsilon$ turbulence model could only predict the generation of main vortices, but it fails at predicting any induced vortices.

This study highlights the dominance of the SST $\kappa$-$\omega$ turbulence model over the RNG $\kappa$-$\varepsilon$ turbulence model in predicting flow structure characteristics of longitudinal vortices in a parallel plate channel downstream vortex generator. Moreover, the SST $\kappa$-$\omega$ turbulence model can capture accurately the main and induced vortices and therefore it is preferable to be used in CFD studies dedicated for convective heat transfer enhancement using vortex generators.

## References


[1] M. Aris, R. McGlen, I. Owen and C. Sutcliffe, "An experimental investigation into the deployment of 3-D, finned wing and shape memory alloy vortex generators in a forced air convection heat pipe fin stack," *Applied Thermal Engineering,* vol. 31, no. 14-15, pp. 2230-2240, 1 10 2011.

[2] Y. Li, X. Wang, J. Zhang, L. Zhang and J. Wu, "Comparison and analysis of the arrangement of delta winglet pair vortex generators in a half coiled jacket for heat transfer enhancement," *International Journal of Heat and Mass Transfer,* vol. 129, pp. 287-298, 2019.

[3] S. Ali, C. Habchi, S. Menanteau, T. Lemenand and J. Harion, "Three-dimensional numerical study of heat transfer and mixing enhancement in a circular pipe using self-sustained oscillating flexible vorticity generators," *Chemical Engineering Science,* vol. 162, pp. 152-174, 2017.

[4] L. Zhang, X. Yan, Y. Zhang, Y. Feng, Y. Li, H. Meng, J. Zhang and J. Wu, "Heat transfer enhancement by streamlined winglet pair vortex generators for helical channel with rectangular cross section," *Chemical Engineering and Processing - Process Intensification,* vol. 147, p. 107788, 2020.

[5] H. Karkaba, T. Dbouk, C. Habchi, S. Russeil, T. Lemenand and D. Bougeard, "Multi objective optimization of vortex generators for heat transfer enhancement using large design space exploration," *Chemical Engineering and Processing - Process Intensification,* vol. 154, p. 107982, 2020.

[6] C. Habchi and J. Harion, "Residence time distribution and heat transfer in circular pipe fitted with longitudinal rectangular wings," *International Journal of Heat and Mass Transfer,* vol. 74, pp. 13-24, 2014.

[7] M. Khoshvaght-Aliabadi, S. Zangouei and F. Hormozi, "Performance of a plate-fin heat exchanger with vortex-generator channels: 3D-CFD simulation and experimental validation," *International Journal of Thermal Sciences,* vol. 88, pp. 180-192, 2015.

[8] M. Awais and A. A. Bhuiyan, "Heat transfer enhancement using different types of vortex generators (VGs): A review on experimental and numerical activities," *Thermal Science and Engineering Progress,* vol. 5, pp. 524-545, 1 3 2018.

[9] B. Kumar, G. P. Srivastava, M. Kumar and A. K. Patil, "A review of heat transfer and fluid flow mechanism in heat exchanger tube with inserts," *Chemical Engineering and Processing - Process Intensification,* vol. 123, pp. 126-137, 2018.

[10] M. Fiebig, "Embedded Vortices in Internal Flow: Heat Transfer and Pressure Loss Enhancement," *International Journal of Heat and Fluid Flow,* vol. 16, no. 5, pp. 376-388, 1995.

[11] C. Habchi, T. Lemenand, D. Della Valle, M. Khaled, A. Elmarakbi and H. Peerhossaini, "Mixing assessment by chemical probe," *Journal of Industrial and Engineering Chemistry,* vol. 20, pp. 1411-1420, 2014.

[12] M. Oneissi, C. Habchi, S. Russeil, T. Lemenand and D. Bougeard, "Heat transfer enhancement of inclined projected winglet pair vortex generators with protrusions," *International Journal of Thermal Sciences ,* vol. 134, pp. 541-551, 2018.

[13] A. M. Hamed, A. Pagan-Vazquez, D. Khovalyg, Z. Zhang and L. P. Chamorro, "Vortical structures in the near wake of tabs with various geometries," *Journal of Fluid Mechanics,* vol. 825, pp. 167-188, 25 8 2017.

[14] C. M. Velte, M. O. L. Hansen and D. Cavar, "Flow analysis of vortex generators on wing sections by stereoscopic particle image velocimetry measurements," *Environmental Research Letters,* vol. 3, no. 1, p. 015006, 1 2008.

[15] A. Mokrani, C. Castelain and H. Peerhossaini, "Experimental study of the influence of the rows of vortex generators on turbulence structure in a tube," *Chemical Engineering and Processing: Process Intensification,* vol. 48, pp. 659-671, 2009.

[16] G. Lu and X. Zhai, "Effects of curved vortex generators on the air-side performance of fin-and-tube heat exchangers," *International Journal of Thermal Sciences,* vol. 136, pp. 509-518, 2019.

[17] M. Awais and A. A. Bhuiya, "Enhancement of thermal and hydraulic performance of compact finned-tube heat exchanger using vortex generators (VGs): A parametric study," *International Journal of Thermal Sciences,* vol. 140, pp. 154-166, 2019.

[18] A. Khanjian, C. Habchi, S. Russeil, D. Bougeard and T. Lemenand, "Effect of the angle of attack of a rectangular wing on the heat transfer enhancement in channel flow at low Reynolds number," *Heat and Mass Transfer,* p. 1441–1452, 2018.

[19] T. Lemenand, H. C. D. Della Valle and H. Peerhossaini, "Vorticity and convective heat transfer downstream a vortex generator," *International Journal of Thermal Science,* vol. 125, pp. 342-349, 2018.

[20] L. Garelli, G. Ríos Rodriguez, J. J. Dorella and M. A. Storti, "Heat transfer enhancement in panel type radiators using delta-wing vortex generators," *International Journal of Thermal Sciences,* vol. 137, pp. 64-74, 1 3 2019.

[21] A. Gupta, A. Roy, S. Gupta and M. Gupta, "Numerical investigation towards implementation of punched winglet as vortex generator for performance improvement of a fin-and-tube heat exchanger," *International Journal of Heat and Mass Transfer,* vol. 149, p. 119171, 2020.

[22] L. O. Salviano, D. J. Dezan and J. I. Yanagihara, "Optimization of winglet-type vortex generator positions and angles in plate-fin compact heat exchanger: Response Surface

Methodology and Direct Optimization," *International Journal of Heat and Mass Transfer,* vol. 82, pp. 373-387, 2015.

[23] M. Hatami, D. Ganji and M. Gorji-Bandpy, "Experimental and numerical analysis of the optimized finned-tube heat exchanger for OM314 diesel exhaust exergy recovery," *Energy Conversion and Management,* vol. 97, pp. 26-41, 2015.

[24] C. Habchi, S. Russeil, D. Bougeard, J. L. Harion, T. Lemenand, D. Della Valle and H. Peerhossaini, "Enhancing Heat Transfer in Vortex Generator-type Multifunctional Heat Exchangers," *Applied Thermal Engineering,* vol. 38, pp. 14-25, 2012.

[25] X.-Y. Tang and D.-S. Zhu, "Flow structure and heat transfer in a narrow rectangular channel with different discrete rib arrays," *Chemical Engineering and Processing: Process Intensification,* vol. 69, pp. 1-14, 2013.

[26] S. Eiamsa-ard and P. Promvonge, "Numerical study on heat transfer of turbulent channel flow over periodic grooves," *International Communications in Heat and Mass Transfer,* vol. 35, no. 7, pp. 844-852, 2008.

[27] F. Moukalled, L. Mangani and M. Darwish, The Finite Volume Method in Computational Fluid Dynamics, New York City: Springer, 2015.

[28] M. Oneissi, C. Habchi, S. Russeil, D. Bougeard and T. Lemenand, "Novel design of delta winglet pair vortex generator for heat transfer enhancement," *International Journal of Thermal Sciences,* vol. 109, pp. 1-9, 2016.

[29] V. Yakhot and S. Orszag, "Renormalization group analysis of turbulence:(i) basic theory," *Journal of Scientific Computing,* vol. 1, pp. 3-51, 1986.

[30] V. Yakhot, S. Orszag, S. Thangam, T. Gatski and C. Speziale, "Development of turbulence models for shear flows by a double expansion technique," *Physics of Fluids A,* vol. 4, no. 7, pp. 1510-1520, 1992.

[31] B. Launder and D. Spalding, "The numerical computation of turbulent flows," *Computer Methods in Applied Mechanics and Engineering,* vol. 3, no. 2, pp. 269-289, 1974.

[32] D. Choudhury, "Introduction to the Renormalization Group Method and Turbulence Modeling," Fluent Inc, Technical memorandum TM-107, 1993.

[33] F. Menter, "Two-equation eddy-viscosity turbulence models for engineering applications," *AIAA Journal,* vol. 32, pp. 1598-1605, 1994.

[34] I. ANSYS, "Standard and SST k-w Models," in *ANSYS Fluent 15.0 Theory Guide*, April 2009, p. 4.31.

[35] K. Yongsiri, P. Eiamsa-ard, K. Wongcharee and S. Eiamsa-ard, "Augmented heat transfer in a turbulent channel flow with inclined detached-ribs," *Case Studies in Thermal Engineering,* vol. 3, pp. 1-10, 2014.

[36] R. Warming and R. Beam, "Upwind second-order difference schemes and applications in aerodynamic flows," *AIAA Journal,* vol. 14, no. 9, pp. 1241-149, 1976.

[37] J. Štigler, "Introduction of the analytical turbulent velocity profile between two parallel plates," in *18th International Conference on Engineering Mechanics*, Svratka, Czech Republic, 2012.

[38] I. Celik, U. Ghia, P. Roache, C. Freitas, H. Coleman and P. Raad, "Procedure for Estimation and Reporting of Uncertainty Due to Discretization," *Journal of Fluids Engineering,* vol. 130, pp. 078001-1, 2008.

[39] M. Oneissi, E. Bouhoubeiny, S. Russeil, D. Bougeard, T. Lemenand and C. Habchi, "Experimental analysis by stereo-PIV of the development of streamwise vortices downstream of rectangular winglets," *Heat and Mass Transfer,* vol. 56, pp. 2487-2502, 2020.

[40] B. Wang, S. Lee and K. Ho, "Chemical composition of fine particles from incense

burning in a large environmental chamber," *Atmospheric Environment,* vol. 40, pp. 7858-7868, 2006.

[41] Y. Cheng, W. Bechtold, C. Yu and I. Hung, "Incense Smoke: Characterization and Dynamics in Indoor Environments," *Aerosol Science and Technology,* vol. 23, pp. 271-281, 1995.

[42] T. Favelier, M. Michard and N. Grosjean, "Développement d'un critère d'identification de structures tourbillonnaires adapté aux mesures de vitesse par PIV," in *Proc. 9ème Congrès Francophone de Vélocimétrie Laser*, Bruxelles, 2004.

[43] J. Wang and Y. Zhao, "Heat and fluid flow characteristics of a rectangular channel with a small diameter circular cylinder as vortex generator," *International Journal of Thermal Sciences,* vol. 92, p. 2015, 1-13.

[44] A. K. Prasad and K. Jensen, "Scheimpflug stereocamera for particle image velocimetry in liquid flows," *Applied Optics,* vol. 34, no. 30, pp. 7092-7099, 1995.

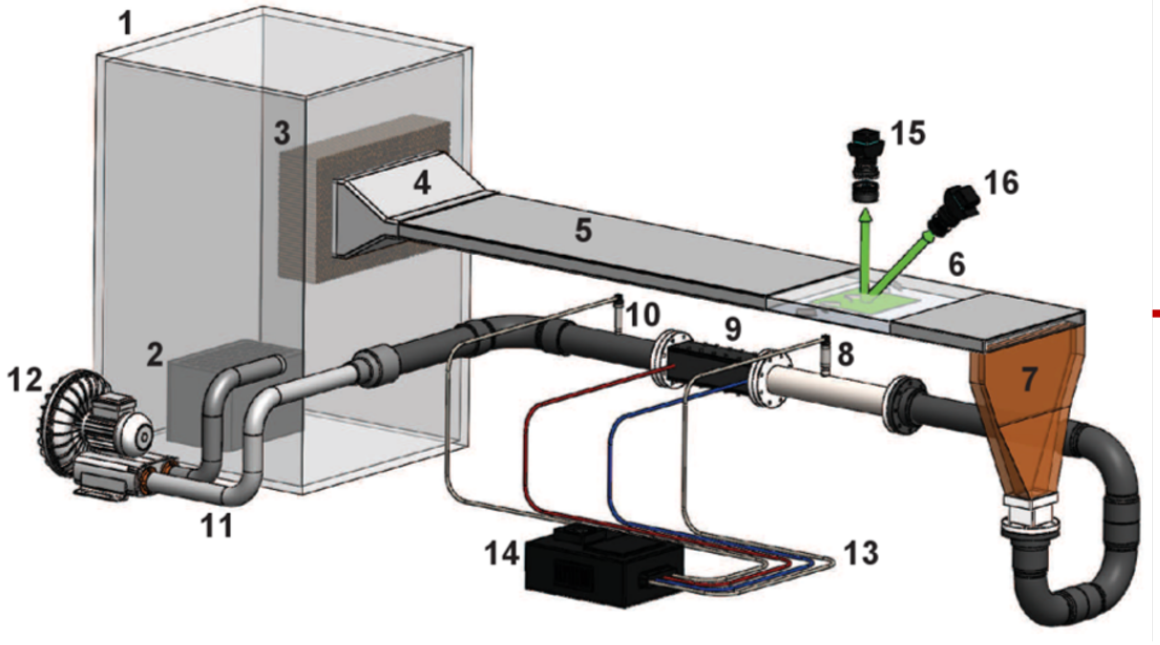


**SPIV and LDV measurements**

**CFD simulations**